

Pattern formation in a thin-film equation with spatially homogeneous and non-homogeneous Derjaguin disjoining pressure

A. S. ALSHAIKHI¹, M. GRINFELD^{1,2} and S. K. WILSON¹

¹ *Department of Mathematics and Statistics, University of Strathclyde, Livingstone Tower, 26 Richmond Street, Glasgow G1 1XH, UK*

² *email: m.grinfeld@strath.ac.uk*

Abstract

We consider pattern formation in a two-dimensional thin film on a planar substrate with a Derjaguin disjoining pressure and periodic wettability stripes in one of the directions. We rigorously clarify some of the results obtained numerically by Honisch *et al.* [*Langmuir* 31: 10618–10631, 2015] and embed them in the general theory of thin-film equations. For the case of constant wettability, we elucidate the change in the global structure of branches of stationary solutions as the average film thickness and the surface tension are varied. Specifically we find, by using methods of local bifurcation theory and the continuation software package AUTO, both nucleation and metastable regimes. We discuss admissible forms of spatially non-homogeneous disjoining pressure, arguing for a form that differs from the one used by Honisch *et al.*, and study the dependence of the stationary solutions on the wettability contrast in that case.

Keywords: thin films, disjoining pressure, non-homogeneous substrates, pattern formation

1 Introduction

Thin liquid films on solid substrates occur in many natural situations. For example, they appear in tear films in the eye which protect the cornea [5] or in streams of lava from a volcanic eruption [15]. Moreover, thin liquid films occur in many technological applications, such as coatings [18] and lubricants (e.g. oil films which lubricate the piston in a car engine [36], drying paint layers [14], and in the manufacture of microelectronic devices [17]). For extensive reviews of thin-film flow see, for example, Oron *et al.* [25] and Craster and Matar [8].

As these liquid films are thin, the Navier–Stokes equation governing their flow can be reduced to a single degenerate fourth-order quasi-linear parabolic partial differential equation usually known as a thin-film equation. In many applications a choice of a disjoining pressure, which we denote by Π , must be made. Such a term describes the action of surface forces on the film [32]. In different situations, different forms of disjoining pressure are appropriate; these may incorporate long-range van der Waals forces and/or various types

of short-range interaction terms such as Born repulsion; inclusion of a particular type of interaction can have significant effects on the wettability of the surface and the evolution of the film, sometimes leading to dewetting phenomena, i.e. the rupture of the film and the appearance of dry spots. (Here and subsequently by “wettability” of the surface we mean the ability of a solid surface to reduce the surface tension of a liquid on contact with it such that it spreads over the surface and wets it.)

Witelski and Bernoff [38] were one of the first authors to analyse mathematically the rupture of three-dimensional thin films. In particular, considering a disjoining pressure of the form $\Pi = -1/(3h^3)$ (we use the sign convention adopted in Honisch *et al.* [13]), they analysed planar and axisymmetric equilibrium solutions on a finite domain. They showed that a disjoining pressure of this form leads to finite-time rupture singularities, that is, the film thickness approaches zero in finite time at a point (or a line or a ring) in the domain. In a related more recent paper, Ji and Witelski [16] considered a different choice of disjoining pressure and investigated the finite-time rupture solutions in a model of thin film of liquid with evaporative effects. They observed different types of finite-time singularities due to the non-conservative terms in the model. In particular, they showed that the inclusion of non-conservative term can prevent the disjoining pressure from causing finite-time rupture.

A pioneering theoretical study of a thin-film equation with a disjoining pressure term given by a combination of negative powers of the height of the thin film is that by Bertozzi *et al.* [3], who studied the formation of dewetting patterns and the rupture of thin liquid films due to long-range attractive and short-range Born repulsive forces, and determined the structure of the bifurcation diagram for stationary solutions, both with and without the repulsive term.

Aiming to quantify the temporal coarsening in a thin film, Glasner and Witelski [11] examined two coarsening mechanisms that arise in dewetting films: mass exchange that influences the breakdown of individual droplets and spatial motion that results in droplet rupture as well as merging events. They provided a simple model with a disjoining pressure which combines the effects of both short- and long-range forces acting on the film. Kitavtsev *et al.* [19] analysed the long-time dynamics of dewetting in a thin-film equation by using a disjoining pressure similar to that used by Bertozzi *et al.* [3]. They applied centre manifold theory to derive and analysed an ordinary differential equation model for the dynamics of dewetting.

The recent article by Witelski [37] presents a review of the various stages of dewetting for a film of liquid spreading on a hydrophobic substrate. Different types of behaviour of the film are observed depending on the form of the disjoining pressure: finite-time singularities, self-similar solutions and coarsening. In particular, he divides the evolution of dewetting processes into three phases: an initial linear instability that leads to finite-time rupture (short time dynamics), which is followed by the propagation of dewetting rims and instabilities of liquid ridges (intermediate time dynamics), and the eventual formation of quasi-steady droplets (long time dynamics).

Most of the previous studies of thin liquid films focussed on films on homogeneous substrates. However, thin liquid films on non-homogeneous chemically patterned substrates are also of interest. These have many practical applications, such as in the construction of microfluidic devices and creating soft materials with a particular pattern [27]. Chemically patterned substrates are an efficient way to obtain microstructures of different shapes by using different

types of substrate patterning [30]. Chemical modification of substrates can also be used to avoid spontaneous breakup of thin films, which is often highly undesirable, as, for example, in printing technology [4, 24].

Due to their many applications briefly described above, films on non-homogeneous substrates have been the object of a number of previous theoretical studies which motivate the present work. To mention some of them, Konnur *et al.* [20] found that in the case of an isolated circular patch with wetting properties different from that of the rest of the substrate that chemical non-homogeneity of the substrate can greatly accelerate the growth of surface instabilities. Sharma *et al.* [31] studied instabilities of a liquid film on a substrate containing a single heterogeneous patch and a substrate with stripes of alternating less and more wettable regions. The main concern of that paper was to investigate how substrate patterns are reproduced in the liquid film, and to determine conditions for best templating.

Thiele *et al.* [34] performed a bifurcation analysis using the continuation software package AUTO [9] to study dewetting on a chemically patterned substrate by solving a thin-film equation with a disjoining pressure, using the wettability contrast as a control parameter. The wettability contrast measures the degree of heterogeneity of the substrate; it is introduced and defined rigorously in (5.1) in Section 5. Honisch *et al.* [13] modelled an experiment in which organic molecules were deposited on a chemically non-homogeneous silicon oxide substrates with gold stripes and discuss the redistribution of the liquid following deposition.

In a recent preprint, Liu and Witelski [23] studied thin films on chemically heterogeneous substrates. They claim that in some applications such as digital microfluidics, substrates with alternate hydrophilic and hydrophobic rectangular areas are better described by a piecewise constant function than by a sinusoidal one. Therefore, in contrast to other studies, including the present one, they study substrates with wettability characteristics described by such a function. Based on the structure of the bifurcation diagram, they divide the steady-state solutions into six distinct but connected branches and show that the only unstable branch corresponds to confined droplets, while the rest of the branches are stable.

In the present work, we build on the work of Thiele *et al.* [34] and Honisch *et al.* [13]. Part of our motivation is to clarify and explain rigorously some of the numerical results reported in these papers. In the sinusoidally striped non-homogeneous substrate case, we offer a justification for using a form of the disjoining pressure that differs from the one used in these two papers. A detailed plan of the paper is given in the last paragraph of Section 2.

2 Problem Statement

Denoting the height of the thin liquid film by $z = h(x, y, t)$, where (x, y, z) are the usual Cartesian coordinates and t is time, Honisch *et al.* [13] consider the thin-film equation

$$h_t = \nabla \cdot \{Q(h)\nabla P(h, x, y)\}, \quad t > 0, \quad (x, y) \in \mathbb{R}^2, \quad (2.1)$$

where $Q(h) = h^3/(3\eta)$ is the mobility coefficient with η being the dynamic viscosity. The generalized pressure $P(h, x, y)$ is given by

$$P(h, x, y) = -\gamma\Delta h - \Pi(h, x, y),$$

where γ is the surface tension and we follow [13] in taking the Derjaguin disjoining pressure $\Pi(h, x, y)$ in the spatially homogeneous case to be of the form

$$\Pi(h, x, y) = -\frac{A}{h^3} + \frac{B}{h^6} \quad (2.2)$$

suggested, for example, by Pismen [26]. Here A and B are positive parameters that measure the relative contributions of the short-range forces (the h^{-6} term) and the long-range ones (the h^{-3} term). However, we will see that both of these constants can be scaled out of the mathematical problem.

In what follows, we study thin films on both homogeneous and non-homogeneous substrates. In the non-homogeneous case, we will modify (2.2) by assuming that the Derjaguin pressure term Π changes periodically in the x -direction with period L . The appropriate forms of Π in the non-homogeneous case are discussed in Section 5.

Hence, in order better to understand solutions of (2.1), we start by characterising y -independent stationary solutions of that equation for $0 < x < L$ subject to periodic boundary conditions at $x = 0$ and $x = L$. In other words, we seek solutions of (2.1) in the form $h(x, y, t) = h(x)$, satisfying in dimensional variables the non-local boundary value problem

$$\gamma h_{xx} + \frac{B}{h^6} - \frac{A}{h^3} - \frac{1}{L} \int_0^L \left[\frac{B}{h^6} - \frac{A}{h^3} \right] dx = 0, \quad 0 < x < L, \quad (2.3)$$

subject to the constraint

$$\frac{1}{L} \int_0^L h(x) dx = h^*, \quad (2.4)$$

where the constant $h^* (> 0)$ denotes the (scaled) average film thickness, and the periodic boundary conditions

$$h(0) = h(L), \quad h_x(0) = h_x(L). \quad (2.5)$$

Now we non-dimensionalise. Setting

$$H = \left(\frac{B}{A} \right)^{1/3}, \quad h = H\tilde{h}, \quad \text{and } x = L\tilde{x},$$

in (2.3) and removing the tildes, we obtain

$$\epsilon^2 h_{xx} + f(h) - \int_0^1 f(h) dx = 0, \quad 0 < x < 1, \quad (2.6)$$

where

$$f(h) = \frac{1}{h^6} - \frac{1}{h^3}, \quad (2.7)$$

and

$$\epsilon^2 = \frac{\gamma B^{4/3}}{L^2 A^{7/3}}, \quad (2.8)$$

subject to the periodic boundary conditions

$$h(0) = h(1), \quad h_x(0) = h_x(1), \quad (2.9)$$

and the volume constraint

$$\int_0^1 h(x) \, dx = \bar{h} := \frac{h^* A^{1/3}}{B^{1/3}}. \quad (2.10)$$

Note that the problem (2.6)–(2.10) is very similar to the corresponding stationary problem for the Cahn–Hilliard equation considered as a bifurcation problem in the parameters \bar{h} and ϵ by Eilbeck *et al.* [10]. The boundary conditions considered in that work were the physically natural double Neumann conditions. The periodic boundary conditions (2.9) in the present problem slightly change the analysis, but our general approach in characterising different bifurcation regimes still follows that of Eilbeck *et al.* [10], though the correct interpretation of the limit as $\epsilon \rightarrow 0_+$ is that now we let the surface tension γ go to zero. In particular, we perform a Liapunov–Schmidt reduction to determine the local behaviour close to bifurcation points and then use AUTO (in the present work we use the AUTO-07p version [9]) to explore the global structure of branches of stationary solutions both for the spatially homogeneous case and for the spatially non-homogeneous case in the case of an x -periodically patterned substrate.

We first investigate the homogeneous case and, having elucidated the structure of the bifurcations of non-trivial solutions from the constant solution $h = \bar{h}$ in that case in Sections 3 and 4, we study forced rotational ($O(2)$) symmetry breaking in the non-homogeneous case in Section 5. In Appendix A, we present a general result about $O(2)$ symmetry breaking in the spatially non-homogeneous case. It shows that in the spatially non-homogeneous case, only two stationary solutions remain from the orbit of solutions of (2.6)–(2.10) induced by its $O(2)$ invariance. We concentrate on the simplest stationary solutions of (2.6)–(2.10), as by a result of Laugesen and Pugh [21, Theorem 1] only such solutions, that is, constant solutions and those having only one extremum point, are linearly stable in the homogeneous case.

Below we use $\|\cdot\|_2$ to denote $L^2([0, 1])$ norms.

3 Liapunov–Schmidt Reduction in the Spatially Homogeneous Case

We start by performing an analysis of the dependence of the global structure of branches of stationary solutions of the problem in the spatially homogeneous case given by (2.6)–(2.10) on the parameters \bar{h} and ϵ .

In what follows, we do not indicate explicitly the dependence of the operators on the parameters \bar{h} and ϵ , and all of the calculations are performed for a fixed value of \bar{h} and close to a bifurcation point $\epsilon = \epsilon_k$ for $k = 1, 2, 3, \dots$ defined below.

We set $v = h - \bar{h}$, so that $v = v(x)$ has zero mean, and rewrite (2.6) as

$$G(v) = 0,$$

where

$$G(v) = \epsilon^2 v_{xx} + f(v + \bar{h}) - \int_0^1 f(v(x) + \bar{h}) \, dx.$$

If we set

$$H = \left\{ w \in C(0,1) : \int_0^1 w(x) dx = 0 \right\},$$

where G is an operator from $D(G) \subset H \rightarrow H$, then $D(G)$ is given by

$$D(G) = \left\{ v \in C^2(0,1) : v(0) = v(1), v_x(0) = v_x(1), \int_0^1 v(x) dx = 0 \right\}.$$

The linearisation of G at v applied to w is defined by

$$dG(v)w = \lim_{\tau \rightarrow 0} \frac{G(v + \tau w) - G(v)}{\tau}.$$

We denote $dG(0)$ by S , so that S applied to w is given by

$$Sw = \epsilon^2 w_{xx} + f'(\bar{h})w. \quad (3.1)$$

To locate bifurcation points, we have to find the nontrivial solutions of the equation $Sw = 0$ subject to

$$w(0) = w(1), \quad w_x(0) = w_x(1). \quad (3.2)$$

The kernel of S is non-empty and two dimensional when

$$\epsilon = \epsilon_k = \frac{\sqrt{f'(\bar{h})}}{2k\pi} \quad \text{for } k = 1, 2, 3, \dots, \quad (3.3)$$

and is spanned by $\cos(2k\pi x)$ and $\sin(2k\pi x)$. That these values of ϵ correspond to bifurcation points follows from two theorems of Vanderbauwhede [35, Theorems 2 and 3, pp. 361–363].

In a neighbourhood of a bifurcation point $(\epsilon_k, 0)$ in (ϵ, v) space, solutions of $G(v) = 0$ on H are in one-to-one correspondence with solutions of the reduced system of equations on \mathbb{R}^2 ,

$$g_1(x, y, \epsilon) = 0, \quad g_2(x, y, \epsilon) = 0, \quad (3.4)$$

for some functions g_1 and g_2 to be obtained through the Liapunov–Schmidt reduction [12].

To set up the Liapunov–Schmidt reduction, we decompose $D(G)$ and H as follows:

$$D(G) = \ker S \oplus M$$

and

$$H = N \oplus \text{range } S.$$

Since S is self-adjoint with respect to the L^2 -inner product denoted by $\langle \cdot, \cdot \rangle$, we can choose

$$M = N = \text{span} \{ \cos(2kx), \sin(2kx) \},$$

and denote the above basis for M by $\{w_1, w_2\}$ and for N by $\{w_1^*, w_2^*\}$. We also denote the projection of H onto $\text{range } S$ by E .

Since the present problem is invariant with respect to the group $O(2)$, the functions g_1 and g_2 must have the form

$$g_1(x, y, \epsilon) = xp(x^2 + y^2, \epsilon), \quad g_2(x, y, \epsilon) = yp(x^2 + y^2, \epsilon), \quad (3.5)$$

for some function $p(\cdot, \cdot)$ [7], which means that in order to determine the bifurcation structure, the only terms that need to be computed are $g_{1,x\epsilon}$ and $g_{1,xxx}$, as these immediately give $g_{2,y\epsilon}$ and $g_{2,yyy}$ and all of the other second and third partial derivatives of g_1 and g_2 are identically zero.

Following Golubitsky and Schaeffer [12], we have

$$g_{1,x\epsilon} = \langle w_1^*, dG_\epsilon(w_1) - d^2G(w_1, S^{-1}EG_\epsilon(0)) \rangle, \quad (3.6)$$

$$g_{1,xxx} = \langle w_1^*, d^3G(w_1, w_1, w_1) - 3d^2G(w_1, S^{-1}E[d^2G(w_1, w_1)]) \rangle, \quad (3.7)$$

where

$$d^r G(z_1, \dots, z_r) = \frac{\partial^r}{\partial t_1 \dots \partial t_r} G(t_1 z_1 + \dots + t_r z_r) \Big|_{t_1 = \dots = t_r = 0} \quad \text{for } r = 1, 2, 3, \dots, \quad (3.8)$$

and we choose

$$w_1 = w_1^* = \cos(2k\pi x),$$

where $w_1 \in \ker S$ and $w_1^* \in (\text{range } S)^\perp$. In particular, from (3.8) we have

$$\begin{aligned} d^2 G(z_1, z_2) &= \frac{\partial^2}{\partial t_1 \partial t_2} G(t_1 z_1 + t_2 z_2) \Big|_{t_1 = t_2 = 0} \\ &= \frac{\partial^2}{\partial t_1 \partial t_2} \left[\epsilon_k(t_1 z_{1,xx} + t_2 z_{2,xx}) + f(t_1 z_1 + t_2 z_2 + \bar{h}) \right. \\ &\quad \left. - \int_0^1 f(t_1 z_1 + t_2 z_2 + \bar{h}) dx \right] \Big|_{t_1 = t_2 = 0} \\ &= f''(\bar{h}) z_1 z_2 - \int_0^1 f''(\bar{h}) z_1 z_2 dx, \end{aligned}$$

and so

$$\begin{aligned} d^2 G(\cos(2k\pi x), \cos(2k\pi x)) &= f''(\bar{h}) \cos^2(2k\pi x) - \int_0^1 f''(\bar{h}) \cos^2(2k\pi x) dx \\ &= f''(\bar{h}) \cos^2(2k\pi x) - \frac{1}{2} f''(\bar{h}). \end{aligned}$$

To obtain $S^{-1}E[d^2G(w_1, w_1)]$, which we denote by $R(x)$, so that $SR = E[d^2G(w_1, w_1)]$, we use the definition of ϵ_k given in (3.3) and solve the second order ordinary differential equation satisfied by $R(x)$,

$$R_{xx} + 4k^2\pi^2 R = 4k^2\pi^2 \frac{f''(\bar{h})}{f'(\bar{h})} \cos^2(2k\pi x) - 2k^2\pi^2 \frac{f''(\bar{h})}{f'(\bar{h})},$$

subject to

$$R(0) = R(1) \quad \text{and} \quad R_x(0) = R_x(1)$$

in $\ker S$. We obtain

$$R(x) = S^{-1}E[d^2G(w_1, w_1)] = -\frac{1}{6} \frac{f''(\bar{h})}{f'(\bar{h})} \cos(4k\pi x),$$

and hence

$$\begin{aligned}
d^2G(w_1, S^{-1}E[d^2G(w_1, w_1)]) &= d^2G\left(\cos(2k\pi x), -\frac{1}{6}\frac{f''(\bar{h})}{f'(\bar{h})}\cos(4k\pi x)\right) \\
&= f''(\bar{h})\cos(2k\pi x)\left(-\frac{1}{6}\frac{f''(\bar{h})}{f'(\bar{h})}\cos(4k\pi x)\right) \\
&\quad - \int_0^1 f''(\bar{h})\cos(2k\pi x)\left(-\frac{1}{6}\frac{f''(\bar{h})}{f'(\bar{h})}\cos(4k\pi x)\right) dx \\
&= -\frac{1}{6}\frac{[f''(\bar{h})]^2}{f'(\bar{h})}\cos(2k\pi x)\cos(4k\pi x). \tag{3.9}
\end{aligned}$$

In addition, from (3.8) we have

$$\begin{aligned}
d^3G(z_1, z_2, z_3) &= \frac{\partial^3}{\partial t_1 \partial t_2 \partial t_3} G(t_1 z_1 + t_2 z_2 + t_3 z_3) \Big|_{t_1=t_2=t_3=0} \\
&= f'''(\bar{h})z_1 z_2 z_3 - \int_0^1 f'''(\bar{h})z_1 z_2 z_3 dx,
\end{aligned}$$

and therefore

$$\begin{aligned}
d^3G(\cos(2k\pi x), \cos(2k\pi x), \cos(2k\pi x)) &= f'''(\bar{h})\cos^3(2k\pi x) - \int_0^1 f'''(\bar{h})\cos^3(2k\pi x) dx \\
&= f'''(\bar{h})\cos^3(2k\pi x). \tag{3.10}
\end{aligned}$$

Putting all of the information in (3.9) and (3.10) into (3.7) we obtain

$$\begin{aligned}
g_{1,xxx} &= \langle w_1^*, d^3G(w_1, w_1, w_1) - 3d^2G(w_1, S^{-1}E[d^2G(w_1, w_1)]) \rangle \\
&= \int_0^1 \cos(2k\pi x) \left[f'''(\bar{h})\cos^3(2k\pi x) - 3\left(-\frac{1}{6}\frac{[f''(\bar{h})]^2}{f'(\bar{h})}\cos(2k\pi x)\cos(4k\pi x)\right) \right] dx \\
&= \frac{3}{8}f'''(\bar{h}) + \frac{1}{8}\frac{[f''(\bar{h})]^2}{f'(\bar{h})}. \tag{3.11}
\end{aligned}$$

In addition, $G_\epsilon(v) = v_{xx}$, so that $G_\epsilon(0) = 0$ at $v = 0$, and hence we have

$$d^2G(w_k, S^{-1}EG_\epsilon(0)) = 0.$$

Furthermore, since $dG_\epsilon(w) = w_{xx}$, from (3.6) we obtain

$$\begin{aligned}
g_{1,x\epsilon} &= \langle w_1^*, dG_\epsilon(w_1) - d^2G(w_1, S^{-1}EG_\epsilon(0)) \rangle \\
&= \int_0^1 \cos(2k\pi x) (-4\pi^2 k^2 \cos(2k\pi x)) dx \\
&= -2k^2\pi^2. \tag{3.12}
\end{aligned}$$

Referring to (3.5) and the argument following that equation, the above analysis shows that as long as $f'(\bar{h}) > 0$ at $\epsilon = \epsilon_k$ a circle of equilibria bifurcates from the constant solution $h \equiv \bar{h}$. The direction of bifurcation is locally determined by the sign of $g_{1,xxx}$ given by (3.11). Hence, using $1/\epsilon$ as the bifurcation parameter, the bifurcation of nontrivial equilibria is supercritical if $g_{1,xxx}$ is negative and subcritical if it is positive.

By finding the values of \bar{h} where $g_{1,xxx}$ given by (3.11) with $f(h)$ given by (2.7) is zero, we finally obtain the following proposition:

Proposition 1. *Bifurcations of nontrivial solutions from the constant solution $h = \bar{h}$ of the problem (2.6)–(2.10) are supercritical if $1.289 < \bar{h} < 1.747$ and subcritical if $1.259 < \bar{h} < 1.289$ or if $\bar{h} > 1.747$.*

Proof The constant solution $h \equiv \bar{h}$ will lose stability as ϵ is decreased only if $f'(\bar{h}) > 0$. i.e. if $-6/\bar{h}^7 + 3/\bar{h}^4 > 0$, for $\bar{h} > 2^{1/3} \approx 1.259$. From (3.11) we have that

$$g_{1,xxx} = \frac{57\bar{h}^6 - 426\bar{h}^3 + 651}{2\bar{h}^9(\bar{h}^3 - 2)},$$

so that $g_{1,xxx} < 0$ if $\bar{h} \in (1.289, 1.747)$ giving the result. \square

For $\bar{h} \leq 2^{1/3}$ there are no bifurcations from the constant solution $h = \bar{h}$. Furthermore, we have the following proposition:

Proposition 2. *The problem (2.6)–(2.10) has no nontrivial solutions when $\bar{h} \leq 1$.*

Proof Assume that such a nontrivial solution exists. Then, since $\bar{h} \leq 1$, its global minimum, achieved at some point $x_0 \in (0, 1)$, must be less than 1. (We may take the point x_0 to be an interior point by translation invariance.) But then

$$\epsilon^2 h_{xx}(x_0) = \int_0^1 f(h) dx - f(h(x_0)) < 0,$$

so the point x_0 cannot be a minimum. \square

4 Two-Parameter Continuation of Solutions in the Spatially Homogeneous Case

To describe the change in the global structure of branches of stationary solutions of the problem (2.6)–(2.10) as \bar{h} and ϵ are varied, we use AUTO [9] and our results are summarised in Figure 1.

As Figure 1 shows, a curve of saddle-node (SN) bifurcations which originates from $\bar{h} \approx 1.289$ at $1/\epsilon \approx 23.432$ satisfies $\bar{h} \rightarrow 1^+$ as $1/\epsilon \rightarrow \infty$, while a curve of SN bifurcations which originates from $\bar{h} \approx 1.747$, $1/\epsilon \approx 13.998$ satisfies $\bar{h} \rightarrow \infty$ as $1/\epsilon \rightarrow \infty$.

Figure 1 identifies three different bifurcation regimes, denoted by I, II and III, with differing bifurcation behaviour occurring in the different regimes, namely (using the terminology of [10] in the context of the Cahn-Hilliard equation):

- a “nucleation” regime for $1 < \bar{h} < 2^{1/3} \approx 1.259$ (Regime I),
- a “metastable” regime for $2^{1/3} < \bar{h} < 1.289$ and $\bar{h} > 1.747$ (Regime II), and
- an “unstable” regime for $1.289 < \bar{h} < 1.747$ (Regime III).

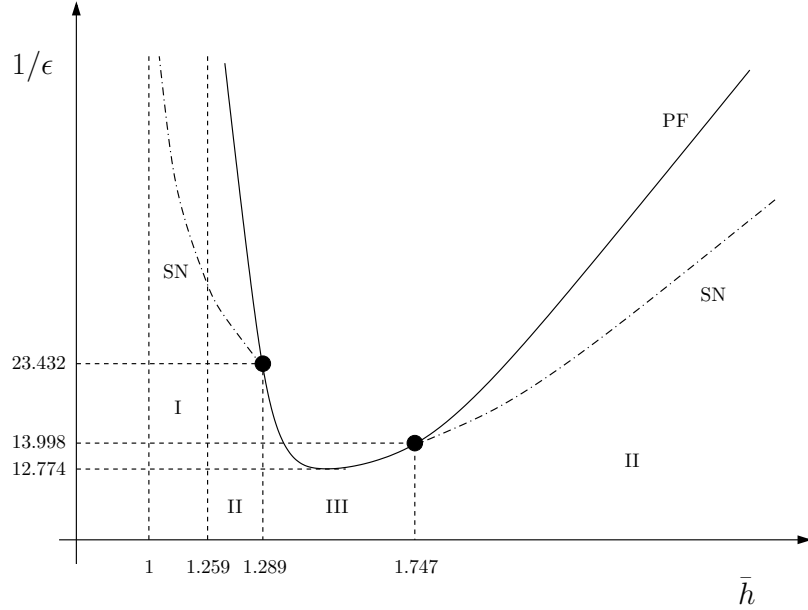


Figure 1: The global structure of branches of stationary solutions with a single maximum, including both saddle-node (SN) (shown with dash-dotted curves) and pitchfork (PF) bifurcation branches (shown with solid curves). The nucleation regime $1 < \bar{h} < 2^{1/3} \approx 1.259$ (Regime I), the metastable regime $2^{1/3} < \bar{h} < 1.289$ and $\bar{h} > 1.747$ (Regime II), and the unstable regime $1.289 < \bar{h} < 1.747$ (Regime III) are also indicated.

In regime I, the constant solution $h(x) \equiv \bar{h}$ is linearly stable which follows from analysing the spectrum of the operator S for $f'(\bar{h}) < 0$ in (3.1) and (3.2), but under sufficiently large perturbations the system will evolve to a non-constant stationary solution.

In regime II, as ϵ is decreased the constant solution $h(x) \equiv \bar{h}$ loses stability through a subcritical bifurcation.

In the regime III, as ϵ is decreased the constant solution $h(x) \equiv \bar{h}$ loses stability through a supercritical bifurcation.

5 The Spatially Non-Homogeneous Case

Honisch *et al.* [13] chose the Derjaguin disjoining pressure $\Pi(h, x, y)$ to be of the form

$$\Pi(h, x, y) = \left(\frac{1}{h^6} - \frac{1}{h^3} \right) (1 + \rho G(x, y)), \quad (5.1)$$

where the function $G(x, y)$ models the non-homogeneity of the substrate and the parameter ρ , which can be either positive or negative, is called the “wettability contrast”. Following Honisch *et al.* [13], in the remainder of the present work we consider the specific case

$$G(x, y) = \sin(2\pi x) := G(x), \quad (5.2)$$

corresponding to an x -periodically patterned (i.e. striped) substrate.

There are, however, some difficulties in accepting (5.1) as a physically realistic form of the disjoining pressure for a non-homogeneous substrate. The problems arise because the two terms in (5.1) represent rather different physical effects. Specifically, since the $1/h^6$ term models the short-range interaction amongst the molecules of the liquid and the $1/h^3$ term models the long-range interaction, assuming that *both* terms reflect the patterning in the substrate in *exactly the same way* through their dependence on the *same* function $G(x, y)$ does not seem very plausible. Moreover, there are other studies which assume that the wettability of the substrate is incorporated in either the short-range interaction term (see, for example, Thiele and Knobloch [33] and Bertozzi *et al.* [3]) or the long-range interaction term (see, for example, Ajaev *et al.* [1] and Sharma *et al.* [31]), but not both simultaneously. Hence in what follows we will consider the two cases $\Pi(h, x) = \Pi_{\text{LR}}(h, x)$ and $\Pi(h, x) = \Pi_{\text{SR}}(h, x)$, where LR stands for “long range” and SR stands for “short range” where

$$\Pi_{\text{LR}}(h, x) = \frac{1}{h^6} - \frac{1}{h^3}(1 + \rho G(x)) \quad (5.3)$$

and

$$\Pi_{\text{SR}}(h, x) = \frac{1}{h^6}(1 + \rho G(x)) - \frac{1}{h^3}, \quad (5.4)$$

in both of which $G(x)$ is given by (5.2) and ρ is the wettability contrast.

For small wettability contrast, $|\rho| \ll 1$, we do not expect there to be significant differences between the influence of Π_{LR} or Π_{SR} of the bifurcation diagrams, as these results depend only on the nature of the bifurcation in the homogeneous case $\rho = 0$ and on the symmetry groups under which the equations are invariant. To see this, consider the spatially non-homogeneous version of (2.6), that is, the boundary value problem

$$\epsilon^2 h_{xx} + f(h, x) - \int_0^1 f(h, x) dx = 0, \quad 0 < x < 1, \quad (5.5)$$

where now

$$f(h, x) = \Pi_{\text{LR}}(h, x) \text{ or } f(h, x) = \Pi_{\text{SR}}(h, x). \quad (5.6)$$

subject to the periodic boundary conditions and the volume constraint,

$$h(0) = h(1), \quad h_x(0) = h_x(1), \text{ and } \int_0^1 h(x) dx = \bar{h}. \quad (5.7)$$

Seeking an asymptotic solution to (5.5)–(5.7) in the form

$$h(x) = \bar{h} + \rho h_1(x) + O(\rho^2)$$

in the limit $\rho \rightarrow 0$, by substituting this ansatz into (5.5) we find that in the case of $\Pi_{\text{LR}}(h, x)$ we have

$$h_1(x) = -\frac{\bar{h}^4 \sin(2\pi x)}{4\pi^2 \bar{h}^7 \epsilon^2 - 3\bar{h}^3 + 6}, \quad (5.8)$$

while in the case of $\Pi_{\text{SR}}(h, x)$ the equivalent result is

$$h_1(x) = \frac{\bar{h} \sin(2\pi x)}{4\pi^2 \bar{h}^7 \epsilon^2 - 3\bar{h}^3 + 6}. \quad (5.9)$$

For non-zero values of ρ , in both the Π_{LR} and Π_{SR} cases, the changes in the bifurcation diagrams obtained in the homogeneous case ($\rho = 0$) are an example of forced symmetry

breaking (see, for example, Chillingworth [6]), which we discuss further in Appendix A. More precisely, we show there that when $\rho \neq 0$, out of the entire $O(2)$ orbit only two equilibria are left after symmetry breaking.

Figure 2 shows how for small wettability contrast $|\rho| \ll 1$, the resulting spatial non-homogeneity introduces imperfections [12] in the bifurcation diagrams of the homogeneous case $\rho = 0$ discussed in Section 4. It presents bifurcation diagrams in regimes I, II and III when the disjoining pressure Π_{LR} is given by (5.3) for a range of small values of ρ together with the corresponding diagrams in the case $\rho = 0$. The corresponding bifurcation diagrams when the disjoining pressure Π_{SR} is given by (5.4) are very similar and hence are not shown here.

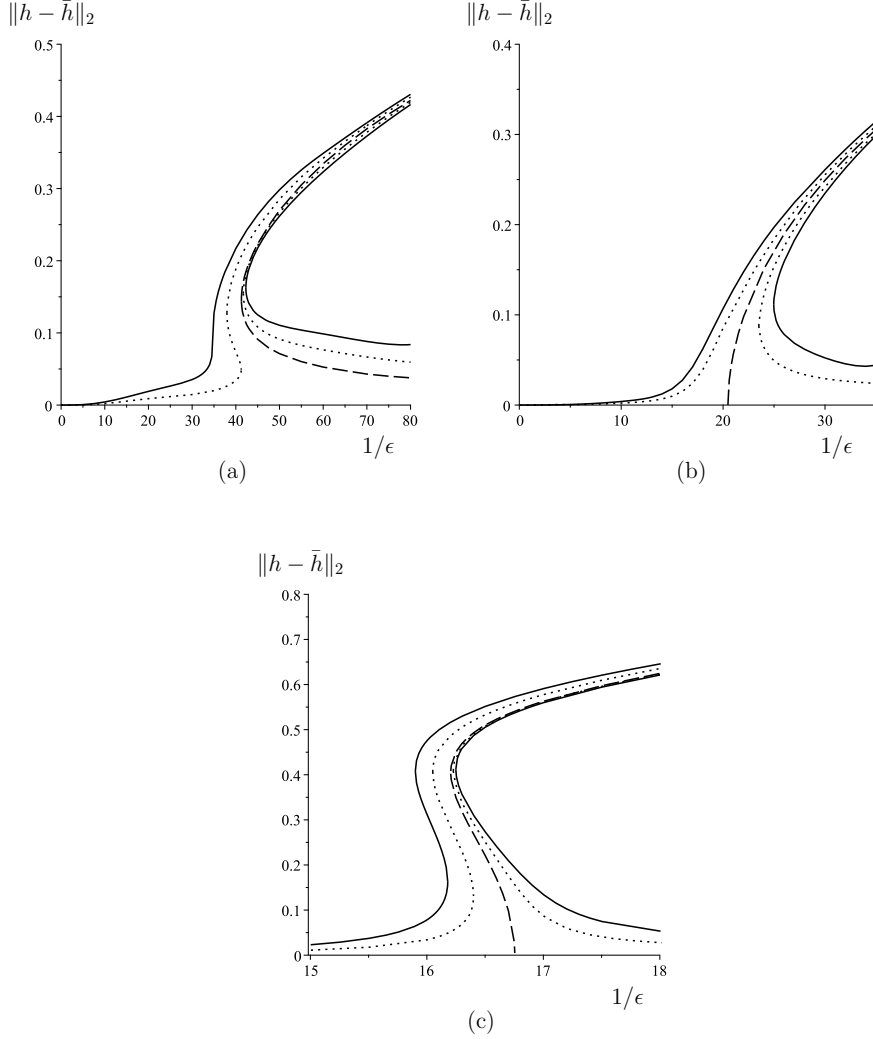


Figure 2: Bifurcation diagrams of solutions with a single maximum, showing $\|h - \bar{h}\|_2$ plotted as a function of $1/\epsilon$ when the disjoining pressure is Π_{LR} for $\rho = 0$ (dashed curves), $\rho = 0.005$ (dotted curves) and $\rho = 0.05$ (solid curves) for (a) $\bar{h} = 1.24$, (b) $\bar{h} = 1.3$, and (c) $\bar{h} = 2$, corresponding to regimes I, II, and III, respectively.

For large wettability contrast, specifically for $|\rho| \geq 1$, significant differences between the two forms of the disjoining pressure are to be expected. When using Π_{LR} , one expects global existence of positive solutions for all values of $|\rho|$; see for example Wu and Zheng [39]. On the other hand, when using Π_{SR} , there is the possibility of rupture of the liquid film for $|\rho| \geq 1$; see for example [3, 39], which means in this case we do not expect positive solutions for sufficiently large values of $|\rho|$.

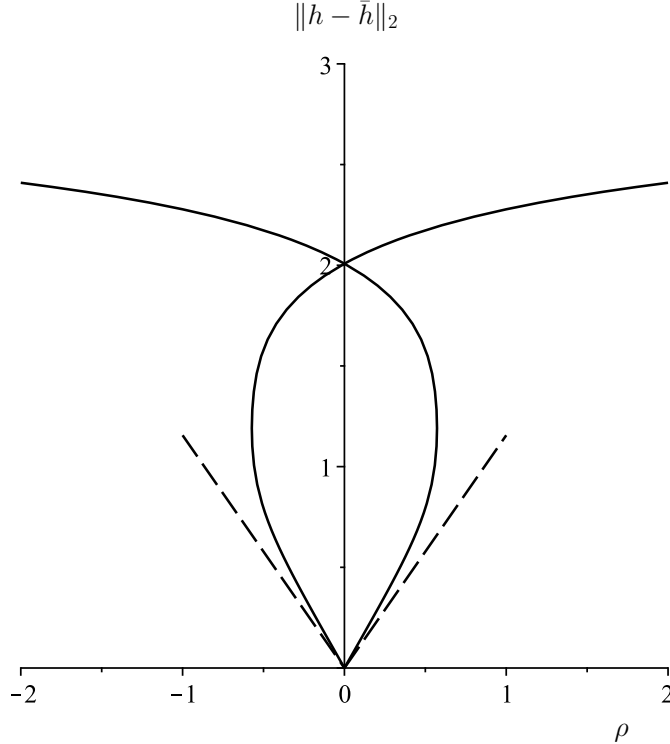


Figure 3: Bifurcation diagram showing $\|h - \bar{h}\|_2$ plotted as a function of ρ when the disjoining pressure is Π_{LR} , $\bar{h} = 3$ and $1/\epsilon = 50$. The leading-order dependence of $\|h - \bar{h}\|_2$ on ρ as $\rho \rightarrow 0$, computed using (5.8) is shown with dashed lines.

In Figure 3 we plot the branches of the positive solutions of (5.5)–(5.7) with a single maximum when the disjoining pressure is Π_{LR} for $\bar{h} = 3$ and $1/\epsilon = 50$, so that when $\rho = 0$, we are in Regime II above the curve PF of pitchfork bifurcations from the constant solution (see Figure 1). The work of Bertozzi [3] and of Wu and Zheng [39], shows that strictly positive solutions exist for all values of $|\rho|$, beyond the range $[-2, 2]$ for which we have performed the continuation.

Figure 4 shows that the situation is different when the disjoining pressure is Π_{SR} (with same \bar{h} and ϵ). At $|\rho| = 1$, one of the branches of smooth solutions disappears due to rupture of the film, so that at some point $x_0 \in [0, 1]$ we have $h = 0$ and a strictly positive solution no longer exists, while the other two branches disappear at a saddle node bifurcation at $|\rho| \approx 5.8$.

Note that in Figures 3 and 4, the non-trivial “solution” on the axis $\rho = 0$ is in fact a whole $O(2)$ -symmetric orbit of solutions predicted by the analysis leading to Figure 1.

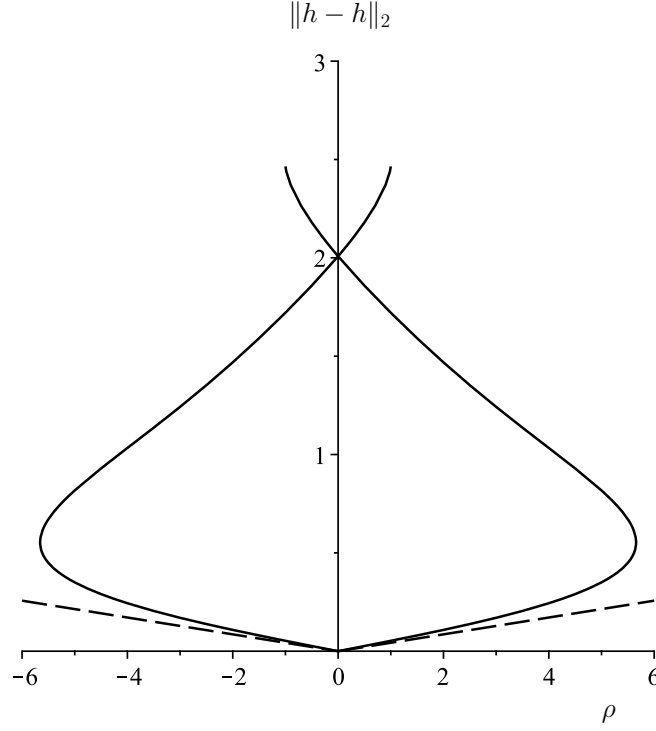


Figure 4: Bifurcation diagram with $\|h - \bar{h}\|_2$ plotted as a function of ρ when the disjoining pressure is Π_{SR} , for $\bar{h} = 3$ and $1/\epsilon = 50$. The leading order dependence of $\|h - \bar{h}\|_2$ on ρ as $\rho \rightarrow 0$, computed using (5.9), is shown with dashed lines.

Note that when the disjoining pressure is Π_{SR} , given by (5.4), we were unable to use AUTO to continue branches of solutions beyond the rupture of the film.

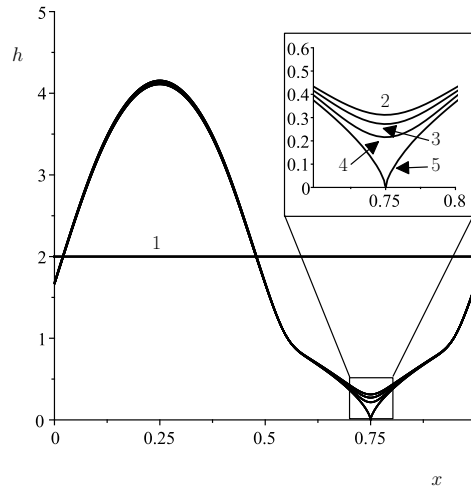


Figure 5: Solutions $h(x)$ when the disjoining pressure is Π_{SR} for $\bar{h} = 2$ and $1/\epsilon = 30$ for $\rho = 0, 0.97, 0.98, 0.99$ and 1 , denoted by “1”, “2”, “3”, “4” and “5”, respectively, showing convergence of strictly positive solutions to a non-strictly positive one as $\rho \rightarrow 1^-$.

Figure 5 shows the film approaching rupture as $\rho \rightarrow 1^-$ at the point where the coefficient of the short-range interaction term disappears when $\rho = 1$, *i.e.* when $1 + \sin(2\pi x) = 0$ and hence at $x = 3/4$. These numerical results are consistent with the arguments of Bertozzi *et al.* [3].

Investigation of the possible leading-order balance in (2.6) when the disjoining pressure is Π_{SR} and $\rho = 1$ in the limit $x \rightarrow 3/4$ reveals that $h(x) = O(x - 3/4)^{2/3}$; continuing the analysis to higher order yields

$$h = (2\pi^2)^{1/3} \left(x - \frac{3}{4}\right)^{2/3} - \frac{4}{27}\epsilon^2 (4\pi^{10})^{1/3} \left(x - \frac{3}{4}\right)^{4/3} + O\left(\left(x - \frac{3}{4}\right)^2\right). \quad (5.10)$$

Figure 6 shows the detail of the excellent agreement between the solution $h(x)$ when $\rho = 1$ and the two-term asymptotic solution given by (5.10) in a neighbourhood of $x = 3/4$.

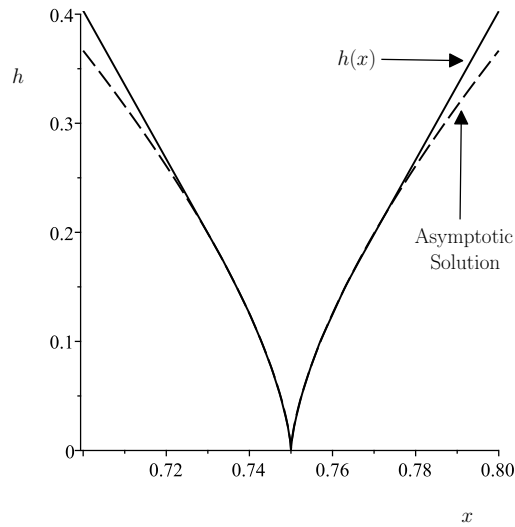


Figure 6: Details near $x = 3/4$ of the solution for $h(x)$ shown with solid line when the disjoining pressure is Π_{SR} and $\rho = 1$, and the two-term asymptotic solution given by (5.10) shown with dashed lines for $\bar{h} = 2$ and $\epsilon = 1/30$.

Finally, Figures 7 and 8 show the multiplicity of solutions with a single maximum for the disjoining pressures Π_{LR} and Π_{SR} , respectively, in the $(1/\epsilon, \rho)$ -plane in the three regimes shown in Figure 1.

In Figure 8 the horizontal dashed line at $\rho = 1$ indicates rupture of the film and loss of a smooth strictly positive solution, implying that there are regions in parameter space where no such solutions exist.

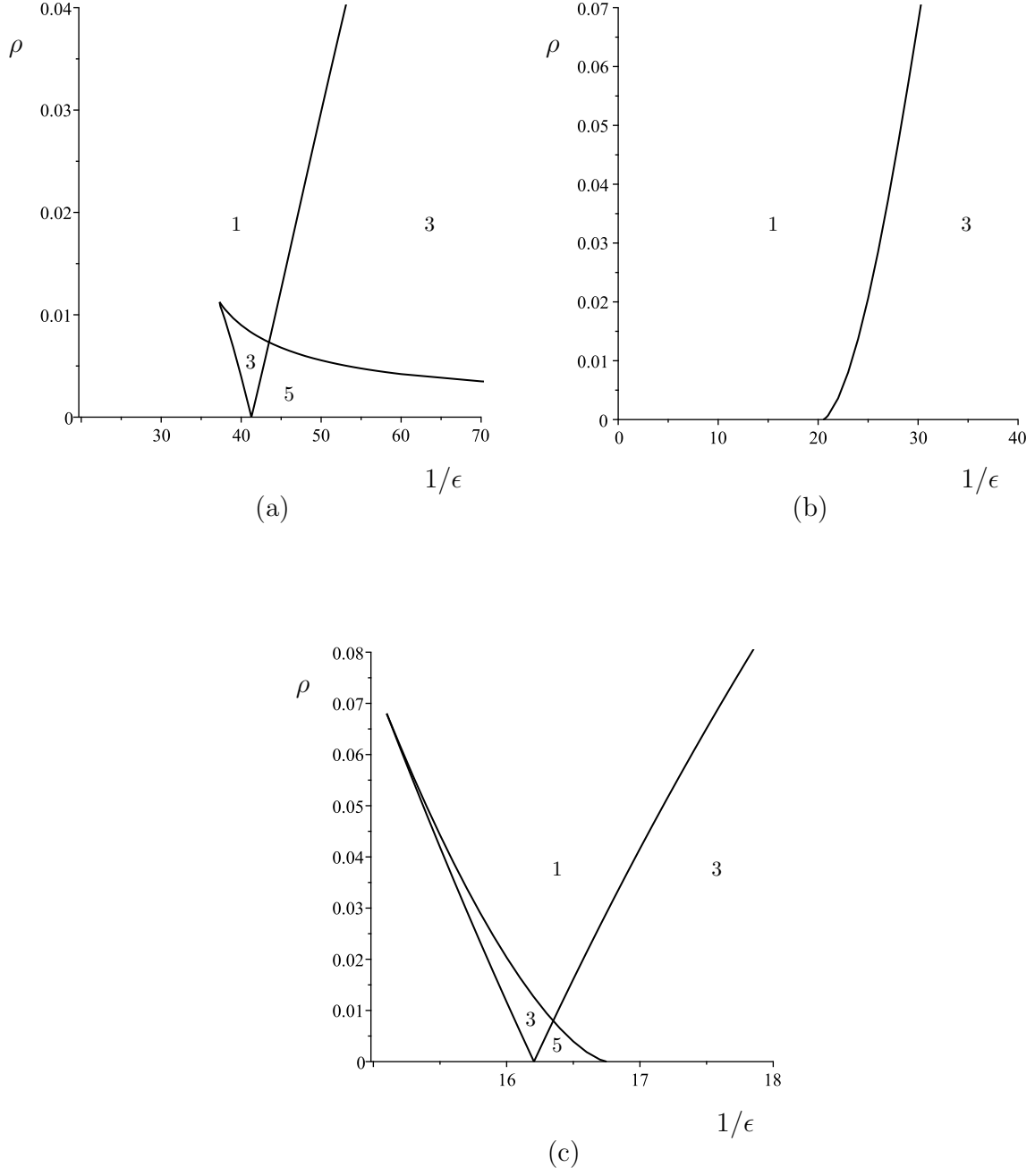


Figure 7: Multiplicity of strictly positive steady state solutions with a single maximum in the $(1/\epsilon, \rho)$ -plane when the disjoining pressure is Π_{LR} for (a) $\bar{h} = 1.24$ (Regime I), (b) $\bar{h} = 1.3$ (Regime II), and (c) $\bar{h} = 2$ (Regime III).

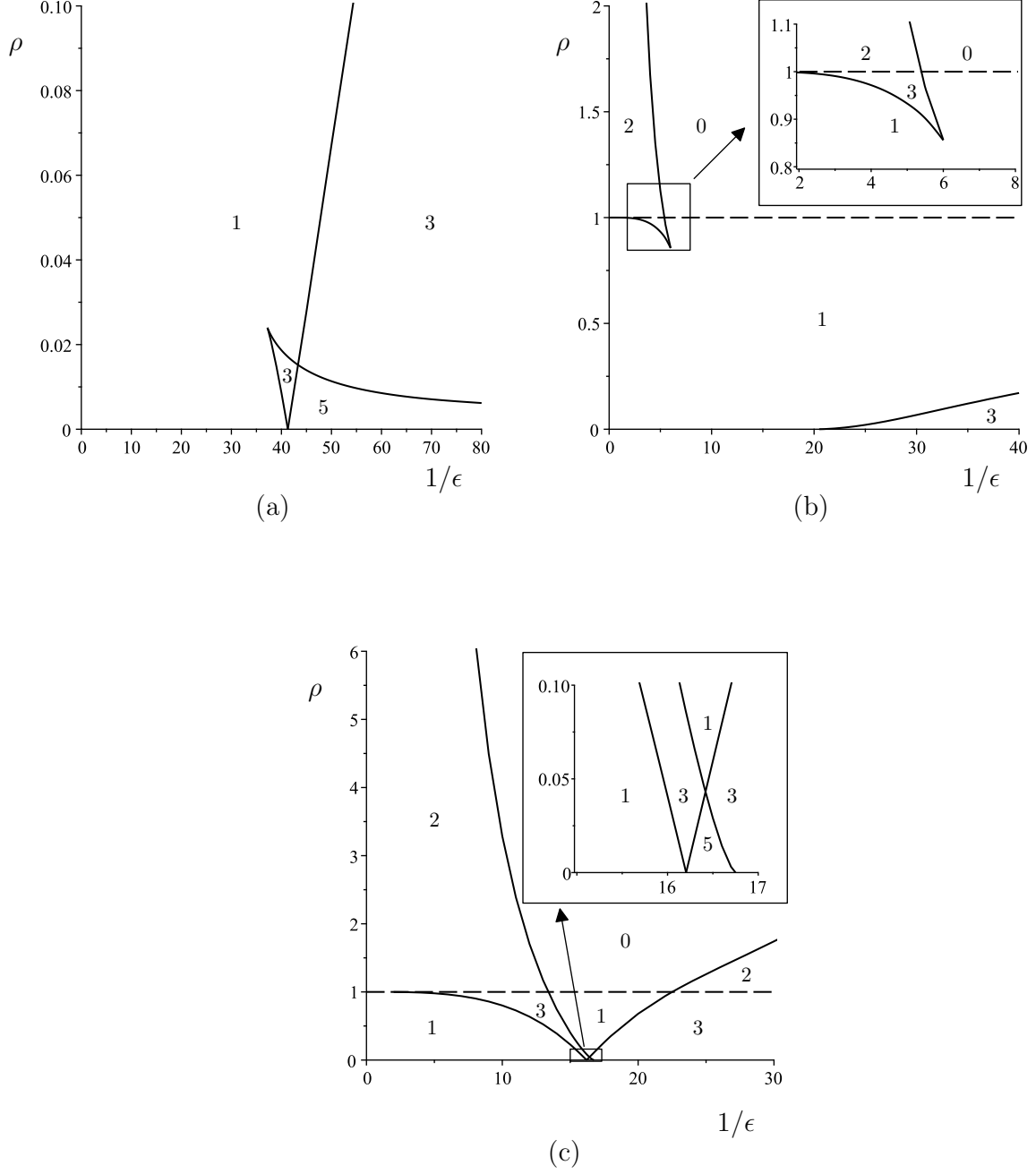


Figure 8: Multiplicity of strictly positive steady state solutions with a single maximum in the $(1/\epsilon, \rho)$ -plane when the disjoining pressure is Π_{SR} for (a) $\bar{h} = 1.24$ (Regime I), (b) $\bar{h} = 1.3$ (Regime II), and (c) $\bar{h} = 2$ (Regime III).

6 Conclusions

In the present work we have investigated the steady state solutions of the thin-film evolution equation (2.1) both in the spatially homogeneous case (2.6)–(2.9) and in the spatially

non-homogeneous case for two choices of spatially non-homogeneous Derjaguin disjoining pressure given by (5.3) and (5.4). We have given a physical motivation for our choices of the disjoining pressure. For reasons explained in the last paragraph of Section 2, we concentrated on branches of solutions with a single maximum.

In the spatially homogeneous case (2.6)–(2.10), we used the Liapunov-Schmidt reduction of an equation invariant under the action of the $O(2)$ symmetry group to obtain local bifurcation results and to determine the dependence of the direction and nature of bifurcation in bifurcation parameter $1/\epsilon = l$ on the average film thickness \bar{h} ; our results on the existence of three different bifurcation regimes, (namely nucleation, metastable, and unstable) are summarised in Propositions 1 and 2 and in the phase diagram shown in Figure 1 obtained using AUTO.

In the spatially non-homogeneous case (5.5)–(5.7), we clarified the $O(2)$ symmetry breaking phenomenon (see Appendix A) and presented imperfect bifurcation diagrams in Figure 2 and global bifurcation diagrams using the wettability contrast ρ as a bifurcation parameter for fixed ϵ and \bar{h} in Figures 3 and 4.

Our results can be described using the language of global compact attractors [39]. Let us discuss Figure 3 in more detail; it is reproduced in Figure 9 with labelling added to the different branches of strictly positive steady state solutions with a single maximum. Below we explain what these different labels mean.

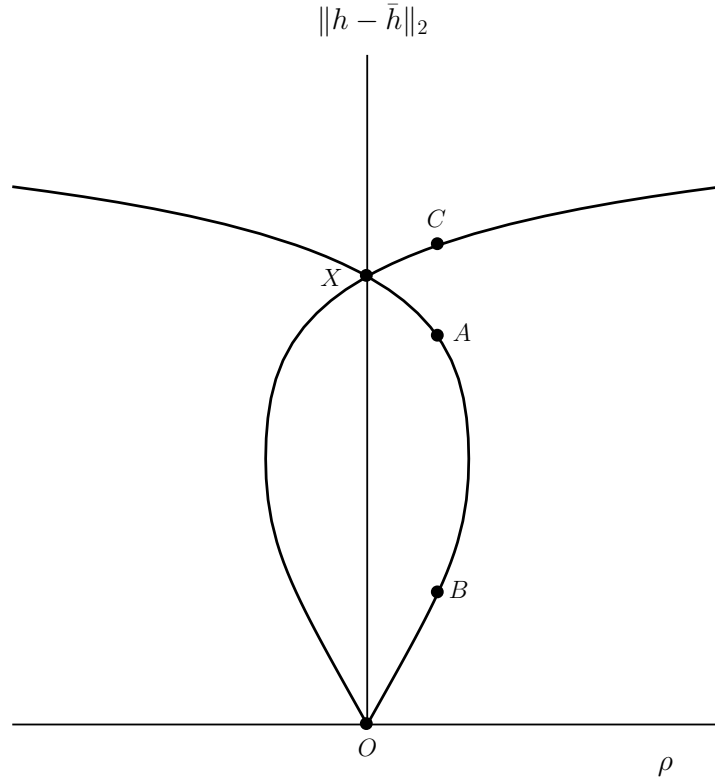


Figure 9: Figure 3 with the different solution branches labelled.

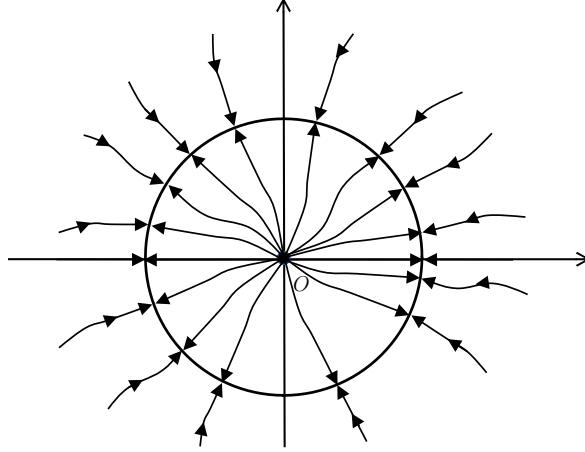


Figure 10: Sketch of the global attractor for $\rho = 0$. The thicker circle represents the $O(2)$ orbit of steady states and O represents the constant solution $h(x) = \bar{h}$.

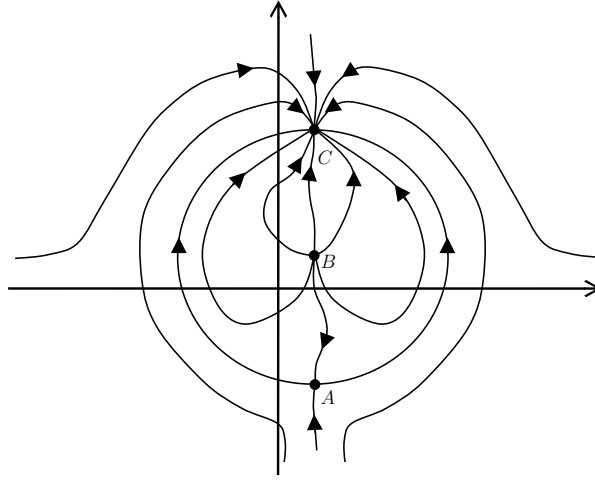


Figure 11: Sketch of the global attractor for small non-zero values of $|\rho|$. The points A , B , C correspond to the steady state solutions labelled in Figure 9.

When $\rho = 0$, for $1/\epsilon = 50$, the attractor is two-dimensional; the constant state $h \equiv \bar{h}$ denoted by O has a two-dimensional unstable manifold and X corresponds to a whole $O(2)$ orbit of steady state solutions. A sketch of the attractor in this case is shown in Figure 10.

When $|\rho|$ takes small positive values, only two steady state solutions, denoted by A and C remain from the entire $O(2)$ orbit, as discussed in Appendix A, while the constant steady state continues to B without change of stability. The resulting two-dimensional attractor is sketched in Figure 11.

Increasing $|\rho|$ causes equilibria B and C to collide in a saddle node bifurcation and disappear, so that the attractor degenerates to a single asymptotically stable equilibrium. It would be interesting to understand why this collision of equilibrium branches has to occur.

We have also explored the geometry of film rupture which occurs as $\rho \rightarrow 1^-$ when the disjoining pressure is given by Π_{SR} ; this phenomenon is shown in detail in Figures 5 and 6.

Finally, in Figures 7 and 8, we showed the results of a two-parameter continuation study in the $(1/\epsilon, \rho)$ plane, showing how the multiplicity of positive steady state solutions changes as parameters are varied, and in particular, indicating in the case of Derjaguin pressure Π_{SR} shown in Figure 8 regions in parameter space where no such solutions exist. We conjecture that in these regions the solution of the unsteady problem with any positive initial condition converges to a weak solution of the thin-film equation with regions in which $h(x) = 0$, i.e. solutions with film rupture (dry spots). For a discussion of such (weak) solutions of thin-film equations in the homogeneous case the reader is referred to the work of Laugesen and Pugh [22].

In the case of disjoining pressure (5.4), we could not use the AUTO-07p version of AUTO to continue branches of solutions beyond touchdown. It would be an interesting project to develop such a capability for this powerful and versatile piece of software.

Figures 8(b) and 8(c) provide numerical evidence for the existence of a curve of saddle-node bifurcations converging to the point $(0, 1)$ in the $(1/\epsilon, \rho)$ plane; an explanation for this feature of the global bifurcation diagrams requires further study.

To summarise: our study was primarily motivated by [13]. While we have clarified the mathematical properties of (2.6)–(2.9) and (5.5)–(5.7), so that the structure of bifurcations in Figure 3(a) of that paper for non-zero values of ρ is now understood, many of their other numerical findings are still to be explored mathematically, for example, the stability of ridge solutions shown in their Figure 5.

A final remark that might be of interest to the reader is that the solutions of equations (5.5) – (5.7) are the steady state solutions of the one-dimensional spatially inhomogeneous version of the evolution equation (2.1), which is a degenerate quasi-linear fourth order equation of the form

$$h_t = (Q(h)P(x, h)_x)_x, \quad 0 < x < L. \quad (6.1)$$

These solutions can also be thought of as the steady state solutions of a much simpler (Rubinstein-Sternberg type [28]), second order semi-linear non-local equation,

$$h_t = \gamma h_{xx} + \Pi(h, x) - \frac{1}{L} \int_0^L \Pi(h, x) dx, \quad 0 < x < L. \quad (6.2)$$

It would be interesting to compare the dynamics of (6.1) and (6.2), for example using the spectral comparison principles of Bates and Fife [2].

Acknowledgement

We are grateful to Prof. U. Thiele (University of Münster) for clarifications concerning the work of Honisch *et al.* [13] and for sharing with us the AUTO codes used in that work which formed the basis of our continuation analysis.

A $O(2)$ Symmetry Breaking by Spatial Non-homogeneity

In this Appendix, we present an argument that shows that when the wettability contrast is present, i.e. when $\rho \neq 0$, the breaking of the $O(2)$ symmetry which equation (5.5) with the periodic boundary conditions (5.7) has for $\rho = 0$, leaves only two stationary solutions.

This is, in principle, a known result (see, for example, Chillingworth [6]), but, since we are not aware of an easily accessible reference, we give the details here. As before, we set $G(x) = \sin(2\pi x)$. We provide the proof for Π_{SR} given by (5.4), the proof for Π_{LR} given by (5.3) is similar.

For the case of Π_{SR} , let us rewrite the boundary value problem (5.5) in the form

$$\epsilon^2 h_{xx} + f_1(h) + \rho f_2(h)G(x) - \int_0^1 [f_1(h) + \rho f_2(h)G(x)] dx = 0, \quad 0 < x < 1, \quad (\text{A.1})$$

where

$$f_1(h) = \frac{1}{h^6} - \frac{1}{h^3},$$

and

$$f_2(h) = \frac{1}{h^6},$$

i.e. we separate the spatially homogeneous and spatially non-homogeneous components of the disjoining pressure. Equation (A.1) is subject to the periodic boundary conditions (5.7).

Suppose that when $\rho = 0$ there is an orbit of stationary solutions, i.e. a continuous closed curve of solutions $h_{0,s}(x)$, parameterised by $s \in \mathbb{R}/[0, 1]$, such that $h_{0,s}(x) := h_0(x + s)$, for some function $h_0(x)$, i.e. all these solutions are related by translation. We aim to understand what remains of this orbit for small non-zero ρ .

Fix $s \in \mathbb{R}/[0, 1]$. We write

$$h(x) = h_{0,s}(x) + \rho h_1(x) + O(\rho^2).$$

Substituting this expansion into (A.1) and collecting the $O(\rho)$ terms, we have

$$\begin{aligned} \epsilon^2 h_{1,xx} + (f'_1(h_{0,s}) + f'_2(h_{0,s}))h_1 - \int_0^1 [f'_1(h_{0,s}) + f'_2(h_{0,s})] h_1 dx = \\ - f_2(h_{0,s})G + \int_0^1 f_2(h_{0,s})G dx = 0, \end{aligned} \quad (\text{A.2})$$

where, just like $h_{0,s}(x)$, $h_1(x)$ also satisfies the periodic boundary conditions (5.7).

Now set

$$Ku := \epsilon^2 u_{1,xx} + (f'_1(h_{0,s}) + f'_2(h_{0,s}))u - \int_0^1 [f'_1(h_{0,s}) + f'_2(h_{0,s})]u dx,$$

and let $D(K)$, the domain of K , be

$$D(K) = \{f \in C^2([0, 1]) \mid f(0) = f(1), f'(0) = f'(1)\}.$$

The operator K is self-adjoint with respect to the $L^2([0, 1])$ inner product. Invoking the Fredholm Alternative [29, Theorem 7.26], we conclude that (A.2) has 1-periodic solutions if and only if the right-hand side of (A.2) is orthogonal in $L^2([0, 1])$ to the solutions of $Ku = 0$.

Next, we show that $u := h'_{0,s}$ solves $Ku = 0$. Indeed, by differentiating (A.1) with $\rho = 0$ with respect to x , we find that u solves the equation

$$\epsilon^2 u_{xx} + (f'_1(h_{0,s}) + f'_2(h_{0,s}))u = 0.$$

Integrating this equation over the interval $[0, 1]$, we have that

$$\int_0^1 (f'_1(h_{0,s}) + f'_2(h_{0,s}))u \, dx = 0.$$

Hence

$$\begin{aligned} 0 &= \epsilon^2 u_{xx} + (f'_1(h_{0,s}) + f'_2(h_{0,s}))u \\ &= \epsilon^2 u_{xx} + (f'_1(h_{0,s}) + f'_2(h_{0,s}))u + \int_0^1 (f'_1(h_{0,s}) + f'_2(h_{0,s}))u \, dx = Ku. \end{aligned}$$

Also note that as $h_{0,s}(x)$ satisfies periodic boundary conditions,

$$\int_0^1 h'_{0,s}(x) \, dx = 0. \tag{A.3}$$

Hence the solvability condition for (A.2) is

$$\int_0^1 h'_{0,s}(r) \left[-f_2(h_{0,s})G + \int_0^1 f_2(h_{0,s})G \, dx \right] \, dr = 0. \tag{A.4}$$

By (A.3), this condition reduces to

$$\int_0^1 f_2(h_{0,s})h'_{0,s}G \, dx = 0. \tag{A.5}$$

Now recall that $h_{0,s}(x) = h_0(x + s)$, so if we write $F(x + s) = f_2(h_0(x + s))h'_0(x + s)$, the function $F(\cdot)$ is 1-periodic in x with zero mean. Hence

$$F(z) = \sum_{k=1}^{\infty} \alpha_k \sin(2k\pi z) + \beta_k \cos(2k\pi z).$$

Therefore for $G(x) = \sin(2\pi x)$, the solvability condition for (A.2) becomes

$$\alpha_1 \sin(2k\pi s) - \beta_1 \cos(2\pi s) = 0, \tag{A.6}$$

which has two solutions $s \in \mathbb{R}/[0, 1]$, from which we conclude there is a solution $h_1(x)$ only for two choices of $s \in \mathbb{R}/[0, 1]$, that is, that only two solutions to (A.1) remain from the entire $O(2)$ orbit that exists for $\rho = 0$.

References

- [1] Ajaev, V. S., Gatapova, E. Y. & Kabov, O. A. (2011) Rupture of thin liquid films on structured surfaces. *Physical Review E* **84**, 041606.
- [2] Bates, P. W. & Fife, P. C. (1990) Spectral comparison principles for the Cahn-Hilliard and phase-field equations, and time scales for coarsening. *Physica D: Nonlinear Phenomena* **43**, 335–48.
- [3] Bertozzi, A. L., Grün, G. & Witelski, T. P. (2001) Dewetting films: bifurcations and concentrations. *Nonlinearity* **14**, 1569–92.
- [4] Brasjen, B. J. & Darhuber, A. A. (2011) Dry-spot nucleation in thin liquid films on chemically patterned surfaces. *Microfluidics and Nanofluidics* **11**, 703–16.
- [5] Braun, R. J., King-Smith, P., Begley, C., Li, L. & Gewecke, N. (2015) Dynamics and function of the tear film in relation to the blink cycle. *Progress in Retinal and Eye Research* **45**, 132–64.
- [6] Chillingworth, D. (1985) Bifurcation from an orbit of symmetry. In: Pnevmatikos, S. N. (ed.) *Singularities and Dynamical Systems*. Amsterdam. Elsevier, pp. 285–94.
- [7] Chossat, P. & Lauterbach, R. 2000 *Methods in Equivariant Bifurcations and Dynamical Systems*. Singapore, World Scientific.
- [8] Craster, R. V. & Matar, O. K. (2009) Dynamics and stability of thin liquid films. *Reviews of Modern Physics* **81**, 1131–98.
- [9] Doedel, E. J. & Oldeman, B. E. 2009 *Auto07p: Continuation and Bifurcation for Ordinary Differential Equations*. Montreal. Concordia University.
- [10] Eilbeck, J. C., Furter, J. E. & Grinfeld, M. (1989) On a stationary state characterization of transition from spinodal decomposition to nucleation behaviour in the Cahn–Hilliard model of phase separation. *Physics Letters A* **135**, 272–75.
- [11] Glasner, K. B. & Witelski, T. P. Collision versus collapse of droplets in coarsening of dewetting thin films. *Physica D: Nonlinear Phenomena* **209**, 80–104.
- [12] Golubitsky, M. & Schaeffer, D. G. 1985 *Singularities and Groups in Bifurcation Theory, Vol. I*. New York. Springer.
- [13] Honisch, C., Lin, T.-S., Heuer, A., Thiele, U. & Gurevich, S. V. (2015) Instabilities of layers of deposited molecules on chemically stripe patterned substrates: ridges versus drops. *Langmuir* **31**, 10618–31.
- [14] Howison, S. D., Moriarty, J. A., Ockendon, J. R., Terrill, E. L. & Wilson, S. K. (1997) A mathematical model for drying paint layers. *Journal of Engineering Mathematics* **32**, 377–94.
- [15] Huppert, H. E. (1982) The propagation of two-dimensional and axisymmetric viscous gravity currents over a rigid horizontal surface. *Journal of Fluid Mechanics* **121**, 43–58.

- [16] Ji, H. & Witelski, T. P. (2017) Finite-time thin film rupture driven by modified evaporative loss. *Physica D: Nonlinear Phenomena* **342**, 1–15.
- [17] Karnaushenko, D., Kang, T., Bandari, V. K., Zhu, F. & Schmidt, O. G. (2020) 3D Self-assembled microelectronic devices: concepts, materials, applications. *Advances in Materials* **32**, 1902994.
- [18] Kistler, S. F. & Schweizer, P. M. (eds). 1997 *Liquid Film Coating: Scientific Principles and Their Technological Implications*. New York. Chapman & Hall.
- [19] Kitavtsev, G., Lutz, R. & Wagner, B. (2011) Centre manifold reduction approach for the lubrication equation. *Nonlinearity* **24**, 2347–69.
- [20] Konnur, R., Kargupta, K. & Sharma, A. (2000) Instability and morphology of thin liquid films on chemically heterogeneous substrates. *Physical Review Letters* **84**, 931–34.
- [21] Laugesen, R. S. & Pugh, M. C. (2000a) Linear stability of steady states for thin film and Cahn-Hilliard type equations. *Archive for Rational Mechanics and Analysis* **154**, 3–51.
- [22] Laugesen, R. S. & Pugh, M. C. (2000b) Properties of steady states for thin film equations. *European Journal of Applied Mathematics* **11**, 293–351.
- [23] Liu, W. & Witelski, T. P. (2020) Steady-states of thin film droplets on chemically heterogeneous substrates. *arXiv preprint arXiv:2002.11286*.
- [24] Ondarçuhu, T. & Aimé, J. P. 2013 *Nanoscale Liquid Interfaces: Wetting, Patterning and Force Microscopy at the Molecular Scale*. Stanford. Pan.
- [25] Oron, A., Davis, S. H. & Bankoff, S. G. (1997) Long-scale evolution of thin liquid films. *Reviews of Modern Physics* **69**, 931–80.
- [26] Pismen, L. M. (2002) Mesoscopic hydrodynamics of contact line motion. *Colloids and Surfaces A* **206**, 11–30.
- [27] Quake, S. R. & Scherer, A. (2000) From micro-to nanofabrication with soft materials. *Science* **290**, 1536–40.
- [28] Rubinstein, J. & Sternberg, P. (1992) Nonlocal reaction–diffusion equations and nucleation. *IMA Journal of Applied Mathematics* **48**, 249–64.
- [29] Rynne, B. P. & Youngson, M. A. 2008 *Linear Functional Analysis*, 2nd edition. Berlin. Springer.
- [30] Sehgal, A., Ferreiro, V., Douglas, J. F., Amis, E. J. & Karim, A. (2002) Pattern-directed dewetting of ultrathin polymer films. *Langmuir* **18**, 7041–48.
- [31] Sharma, A., Konnur, R., & Kargupta, K. (2003) Thin liquid films on chemically heterogeneous substrates: self-organization, dynamics and patterns in systems displaying a secondary minimum. *Physica A: Statistical Mechanics and its Applications* **318**, 262–78.

- [32] Starov, V. M. (2013) Disjoining pressure. In: Li, D. (ed). *Encyclopedia of Microfluidics and Nanofluidics*. Berlin. Springer.
- [33] Thiele, U. & Knobloch, E. (2006) On the depinning of a driven drop on a heterogeneous substrate. *New Journal of Physics* **8**, 313.
- [34] Thiele, U., Brusch, L., Bestehorn, M. & Bär, M. (2003) Modelling thin-film dewetting on structured substrates and templates: bifurcation analysis and numerical simulations. *European Physical Journal E* **11** 255–71.
- [35] Vanderbauwhede, A. (1981) Symmetry and bifurcation from multiple eigenvalues. In: Everitt, W. N. & Sleeman, B. D. (eds). *Ordinary and Partial Differential Equations*, Berlin. Springer, pp. 356–65.
- [36] Wang, D., Song, Y., Tian, J., Shigu, E. & Haidak, G. (2018) Research on the fluid film lubrication between the piston-cylinder interface. *AIP Advances* **8**, 105330.
- [37] Witelski, T. P. (2020) Nonlinear dynamics of dewetting thin films. *AIMS Mathematics* **5** 4229.
- [38] Witelski, T. P. & Bernoff, A. J. (2000) Dynamics of three-dimensional thin film rupture. *Physica D: Nonlinear Phenomena* **147**, 155–76.
- [39] Wu, H. & Zheng, S. (2007) Global attractor for the 1-D thin film equation. *Asymptotic Analysis* **51**, 101–11.
- [40] Xue, L., Zhang, J. & Han, Y. (2012) Phase separation induced ordered patterns in thin polymer blend films. *Progress in Polymer Science* **37**, 564–94.